JPE 18-4-5

https://doi.org/10.6113/JPE.2018.18.4.997
ISSN(Print): 1598-2092 / ISSN(Online): 2093-4718

Single-Phase Transformerless PV Power Conditioning Systems with Low Leakage Current and Active Power Decoupling Capability

Hoang Vu Nguyen*, Do-Hyeon Park**, and Dong-Choon Lee†

†,*Department of Electrical Engineering, Yeungnam University, Gyeongsan, Korea
**Research Team, LC TEK Co. Ltd., Gumi, Korea

Abstract

This paper proposes a transformerless photovoltaic (PV) power converter system based on the DC/AC boost inverter, which can solve the leakage current and second-order ripple power issues in single-phase grid-connected PV inverters. In the proposed topology, the leakage current can be decreased remarkably since most of the common-mode currents flow through the output capacitor, by-passing parasitic capacitors, and grounding resistors. In addition, the inherent ripple power component in the single-phase grid inverter can be suppressed without adding any extra components. Therefore, bulky electrolytic capacitors can be replaced by small film capacitors. The effectiveness of the proposed topology has been verified by simulation and experimental results for a 1-kW PV PCS.

Key words: Active power decoupling, Boost inverter, Leakage reduction, PV inverter

I. INTRODUCTION

Recently, solar energy has become one of the fastest growing renewable energy sources [1]. In 2016, the global PV market reached 74.4 GW [2]. PV inverters play an important role in extracting power from PV modules and interfacing with the grid, which can be classified into transformerless systems and galvanic isolation systems. For low power single-phase systems (up to 5 kW), transformerless PV inverters have become more widespread due to their high efficiency, low cost, small volume and light-weight [3]. In such systems, however, due to the parasitic capacitance between the PV panels and the ground, the leakage current may flow through a conducting path consisting of the PV panel, parasitic capacitors, inverter and the grid. This leakage current increases power losses and distorts the grid current. Furthermore, it induces electromagnetic interference and incurs personal safety problems [4], [5]. Therefore, the leakage current needs to be carefully handled to comply with standards and to improve the reliability of PV systems. If the leakage current is over 300 mA, PV inverters should be disconnected from the power grid within 3s [6].

Several topologies have been suggested to solve the issue of leakage currents for single-phase transformerless PV systems [7]-[10]. Among them, the simplest method is to use a full-bridge inverter with bipolar PWM, where the common-mode voltage disappears [11]. However, bipolar PWM causes large ripple currents and high switching losses, which lead to a reduction of the inverter efficiency. A similar approach has been suggested in [9], where the PV panel terminal is directly connected to the ground of the AC grid. Thus, the high-frequency common-mode voltage is zero, resulting in no leakage current. This concept can be implemented by half-bridge topologies such as two-level half-bridge inverters, neutral-point clamped (NPC) inverters, and T-type NPC inverters. However, these circuits require a high DC input voltage, which is the main drawback of these approaches. Another solution is to disconnect the PV array from the grid during a certain operating interval of the inverter. The full-bridge inverter is used for this concept, where the PV panel is isolated from the grid during the freewheeling interval. This can be applied to the DC side or AC side of the full-bridge inverter by adding additional components, such as

Manuscript received Sep. 21, 2017; accepted Feb. 13, 2018
Recommended for publication by Associate Editor Joung-Hu Park.
†Corresponding Author: dclee@yu.ac.kr
Tel: +82-53-810-2582, Fax: +82-53-810-4767, Yeungnam University
*Department of Electrical Engineering, Yeungnam University, Korea
**Research Team, LC TEK Co. Ltd., Korea

the H5 inverter from SMA, and the HERIC inverter from Sunways [12], [13]. Although these topologies can significantly decrease leakage current, additional devices are required, which increases the system complexity, cost, and power losses. In addition, the reliability and lifetime of systems are deteriorated due to the addition of active devices.

In addition to the leakage current issue, there is another problem of an undesirable second-order power ripple, which is inherent in single-phase grid-connected inverters. This ripple power should be filtered out so that the DC-link voltage can be kept constant. Normally, bulky electrolytic capacitors are used to keep the DC voltage constant. However, this results in a large converter size, which in turn leads to a low power density. Therefore, various active power decoupling circuits have been proposed to remove the ripple power at the DC-link and to reduce the capacitance requirement, by which a small film capacitor can be used at the DC-link [14], [15]. The basic idea is to add an auxiliary circuit, which is connected in either in series or parallel to the primary converter. However, these methods require additional devices, which increase the power losses, cost and complexity of systems. In [16], a transformerless PV power conditioning system for leakage current and pulsating power elimination, which based on the differential buck inverter, was proposed. In this inverter, the DC-link voltage needs to be increased by $\sqrt{2}$ times when compared with that of the conventional H-bridge inverter. Another topology consisting of a boost-coupled half-bridge circuit with four switches was proposed in [17], where the issues of the leakage currents and ripple power in single phase inverters have been solved. As a result, a DC-link capacitor of 45 μF can be used. However, the DC-link voltage is double the grid peak voltage, which is a disadvantage of this topology.

In recent years, single-phase DC-AC boost inverters have been introduced, where the DC input voltage is lower than the peak value of the AC grid voltage [18]-[21]. In addition, to avoid DC current ripple at the DC side, a large DC electrolytic capacitor has been used, which is the main drawback of these circuits. Therefore, several active methods to reduce the second-order harmonic ripple for single-phase boost inverters have been proposed for fuel-cells [22], [23]. However, the leakage current issue has not been considered in these topologies.

This paper is an extended version of [24] with experimental verifications, in which a single-phase transformerless PV power conditioning system based on a boost DC-AC inverter is presented. This system is capable of solving the leakage current and ripple power issues in single-phase grid-connected PV inverters. The leakage current in this topology can be bypassed by introducing a conducting path through the output capacitors of the inverter so that the leakage current does not flow through the parasitic capacitor and grounding resistor. In addition, due to the function of single stage boost conversion, the lower PV voltage of the DC side can directly invert AC without a DC-DC boost converter. Furthermore, the active ripple power in this circuit can be effectively decoupled by properly controlling the output capacitor voltages of the inverter. As a result, the DC-link capacitance is reduced significantly without adding any additional devices. Therefore, a 50-μF small film capacitor can be adopted for a 1-kW PV inverter system instead of a large electrolytic capacitor. Simulation and experimental results have been presented to verify the validity of the proposed PV inverter system.

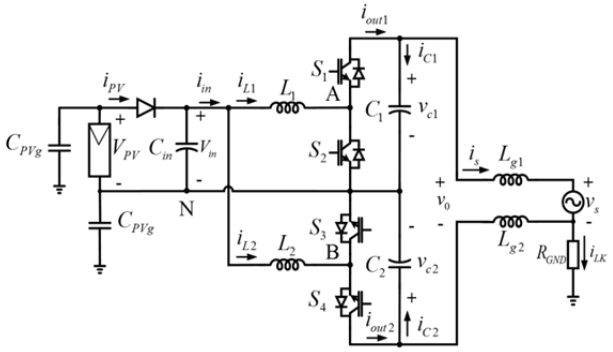

Fig. 1. Single-phase transformerless grid-connected PV system.

II. Proposed Topology with Ripple Power Elimination

A. System Description

Fig. 1 shows the configuration of a single-phase transformerless PV power conditioning system based on the boost DC-AC inverter. The PV inverter consists of two bidirectional boost converters, where output terminals are connected in series, where $C_1 = C_2 = C$ and $L_1 = L_2 = L$ [18]. The inverter is connected to the grid through two inductors L_{g1} and L_{g2}, where $L_{g1} = L_{g2} = L_g / 2$.

Due to its symmetric structure, the operation of the proposed inverter can be simplified as a bidirectional DC-DC converter. Fig. 2 shows the operating modes of the circuit, which includes the discharging mode and the charging mode. When S_1 is turned on and S_2 is turned off, i_{L1} linearly ramps up, and the energy of the inductor is increased. During this mode, the capacitor C_1 is discharged to provide the energy to the grid, as shown in Fig. 2 (a). When S_1 is turned off and S_2 is turned on, the stored energy of the inductor is transferred to the output stage, which consists of the capacitor C_1 and the grid. During this mode, the inductor current i_{L1} decreases, and the capacitor C_1 is recharged, as shown in Fig. 2(b).

B. Analysis of the Active Power Decoupling Function

The function of the inverter is to generate sinusoidal voltage, v_0, which follows the reference voltage:

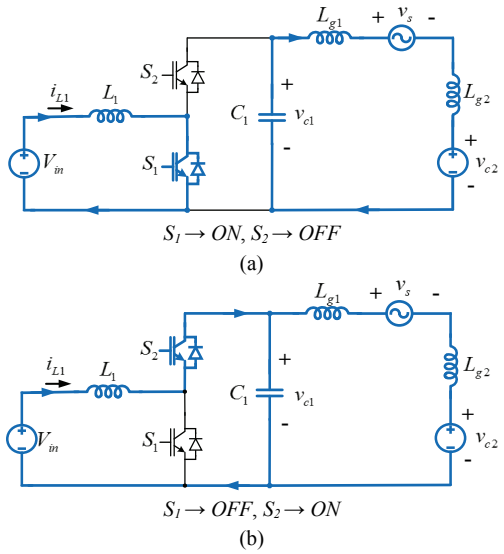

Fig. 2. Operating modes of the circuit. (a) Mode 1. (b) Mode 2.

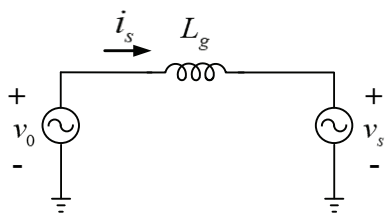

Fig. 3. Equivalent circuit of a grid-connected PV inverter.

$$v_{0,ref} = V_0 \sin(\omega t + \delta) \tag{1}$$

where $V_0, \omega,$ and δ are the amplitude, frequency, and phase angle of the inverter output voltage, respectively. Then the upper and lower capacitor voltages of the inverter need to be controlled to follow their voltage references, respectively, as

$$v_{c1,ref} = V_d + \frac{v_{0,ref}}{2} \tag{2}$$

$$v_{c2,ref} = V_d - \frac{v_{0,ref}}{2} \tag{3}$$

where V_d is the offset in the output capacitor voltages and $V_d > V_{in} + \frac{V_s}{2}$.

Fig. 3 shows an equivalent circuit of the proposed single-phase PV inverter. The grid voltage is assumed to be sinusoidal as

$$v_s = V_s \sin(\omega t) \tag{4}$$

where V_s is the amplitude of the grid voltage.

For a low value of δ, the active and reactive powers exchanged with the grid are expressed, respectively, as

$$P = \frac{V_s V_0}{2\omega L_g}\delta, \tag{5}$$

$$Q = \frac{V_s(V_0 - V_s)}{2\omega L_g}. \tag{6}$$

Therefore, the phase angle δ and inverter voltage amplitude V_0 are used to control the power flow between the inverter and the grid [23]. In this paper, the reactive power is zero due to the unity power factor operation of the inverter, leading to $V_0 = V_s$.

It is assumed that the input current is sinusoidal as

$$i_s = I_s \sin(\omega t) \tag{7}$$

Then the instantaneous output power is expressed as

$$p_s = V_s \sin(\omega t) \times I_s \sin(\omega t) = \frac{V_s I_s}{2} - \frac{V_s I}{2}\cos(2\omega t). \tag{8}$$

It can be seen from (8) that there is a pulsating power component in a single-phase system, which is reflected in the term. In addition, it is possible to individually control the two capacitor voltages of the boost converter such that they can maintain a sinusoidal output voltage waveform, v_0. Therefore, the output capacitor voltages are modified , respectively, as

$$v_{01,ref} = V_d + \frac{V_0}{2}\sin(\omega t + \delta) + B\sin(2\omega t + \theta) \tag{9}$$

$$v_{01,ref} = V_d - \frac{V_0}{2}\sin(\omega t + \delta) + B\sin(2\omega t + \theta) \tag{10}$$

where B is the amplitude and θ is the phase angle of the compensating component. Also, the offset voltage should satisfy the following condition:

$$V_d > V_{in} + \frac{V_s}{2} + B. \tag{11}$$

For the sake of a simple analysis of the active power decoupling function, the effect of the angle δ is neglected. The currents of the capacitors C_1 and C_2 can be derived from (9) and (10) respectively, as

$$i_{C1} = C_1 \frac{dv_{01,ref}}{dt} = C\omega\frac{V_s}{2}\cos(\omega t) + 2C\omega B\cos(2\omega t + \theta) \tag{12}$$

$$i_{C2} = C_2 \frac{dv_{02,ref}}{dt} = -C\omega\frac{V_s}{2}\cos(\omega t) + 2C\omega B\cos(2\omega t + \theta). \tag{13}$$

Then the output currents in leg-A and leg-B are expressed, respectively, as

$$i_{out1} = i_{C1} + i_s = C\omega\frac{V_s}{2}\cos(\omega t) + 2C\omega B\cos(2\omega t + \theta) + I_s\sin(\omega t) \tag{14}$$

$$i_{out2} = i_{C2} - i_s = C\omega\frac{V_s}{2}\cos(\omega t) + 2C\omega B\cos(2\omega t + \theta) - I_s\sin(\omega t). \tag{15}$$

From the voltage and current relationship of the boost inverter, the currents of L_1 and L_2 are calculated, respectively, as

$$i_{L1} = \frac{i_{out1}}{1-d_1} = \frac{i_{out1} v_{C1}}{V_{in}} \tag{16}$$

$$i_{L2} = \frac{i_{out2}}{1-d_2} = \frac{i_{out2} v_{C2}}{V_{in}} \tag{17}$$

where d_1 and d_1 are the duty cycles of the switches, S_2 and S_3, respectively. As shown in Fig. 1, the input current of the PV inverter can be expressed as

$$\begin{aligned} i_{in} &= i_{L1} + i_{L2} \\ &= \frac{V_s I_s + 2B^2 C\omega \sin(4\omega t + \delta) - V_s I_s \cos(2\omega t)}{2V_{in}} \\ &\quad + \frac{0.5 V_s^2 C\omega \sin(2\omega t) + 8 V_d B C\omega \cos(2\omega t + \delta)}{2V_{in}}. \end{aligned} \tag{18}$$

From (18), the input power of the inverter is derived as

$$\begin{aligned} p_{in} &= i_{in} V_{in} \\ &= \frac{V_s I_s + 2B^2 C\omega \sin(4\omega t + \theta) - V_s I_s \cos(2\omega t)}{2} \\ &\quad + \frac{0.5 V_s^2 C\omega \sin(2\omega t) + 8 V_d B C\omega \cos(2\omega t + \theta)}{2}. \end{aligned} \tag{19}$$

It is known from (19) that the input power of the boost inverter has three components; the constant, second-order and fourth-order frequency terms. In order to eliminate the second-order frequency component, the following condition should be satisfied;

$$\begin{aligned} -V_s I_s \cos(2\omega t) + 0.5 V_s^2 C\omega \sin(2\omega t) \\ + 8 V_d B C\omega \cos(2\omega t + \theta) = 0 \end{aligned} \tag{20}$$

Solving (20), the magnitude, *B*, and the phase angle of the compensated component, θ, are obtained, respectively, as

$$\mathrm{B} = \frac{V_s}{8 V_d \omega C} \sqrt{I_s^2 + \omega^2 C^2 V_s^2 / 4} \tag{21}$$

$$\theta = \frac{\pi}{2} - \sin^{-1} \frac{I_s}{\sqrt{I_s^2 + \omega^2 C^2 V_s^2 / 4}}. \tag{22}$$

By controlling the capacitor voltages in (9) and (10) with *B* in (21) and θ in (22), the second-order power ripple of the PV inverter can be mitigated.

III. Analysis of the Leakage Current

A common-mode equivalent circuit of a grid-connected PV inverter in order to analyze the ground leakage current is shown in Fig. 4. It should be noted that the grid voltage is eliminated for a high-frequency analysis since it only contains the fundamental frequency component.

The common-mode voltage, v_{CM}, and common-mode current, i_{CM}, are defined, respectively, as

$$v_{CM} = \frac{v_{AN} + v_{BN}}{2} \tag{23}$$

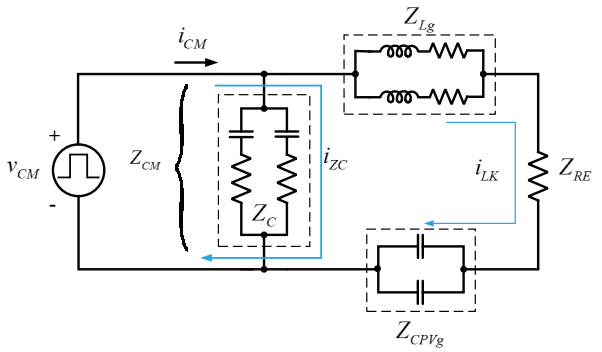

Fig. 4. Equivalent circuit for leakage current analysis of the grid-connected PV inverter.

$$i_{CM} = \frac{v_{CM}}{Z_{CM}} \tag{24}$$

where v_{AN} and v_{BN} are two converter voltages referred to the negative terminal of the DC bus. Z_{CM} is the equivalent common-mode impedance. From Fig. 4, Z_{CM} is obtained as

$$Z_{CM} = \frac{(Z_{Lg} + Z_{RE} + Z_{CPVg}) Z_C}{Z_{Lg} + Z_{RE} + Z_{CPVg} + Z_C} \tag{25}$$

where Z_C, Z_{Lg}, Z_{CPVg}, and Z_E are the impedances of the output capacitor, filter inductor, parasitic capacitor, and ground.

In addition, the equivalent circuit in Fig. 4 shows that the output capacitors, C_1 and C_2, can provide a conducting path for the common-mode current, i_{ZC}, which is given by

$$i_{ZC} = \frac{v_{CM}}{Z_C}. \tag{26}$$

Then by introducing this common-mode conducting path, the leakage current flowing through the parasitic capacitors is expressed as

$$i_{LK} = i_{CM} \frac{Z_C}{Z_{Lg} + Z_{RE} + Z_{CPVg}}. \tag{27}$$

In this topology, the value of the output capacitors is in the microfarad range, while the parasitic capacitors are usually around 100nF for a 1-kW system [16]. Therefore, the impedance of the output capacitors is much lower than those of the parasitic capacitors, grid inductors, and grounding resistor. Therefore, leakage current flows mostly through the output capacitor rather than the grounding resistor and parasitic capacitors. As a result, the leakage current of PV systems is reduced significantly to comply with standards.

IV. Design of the Power Conditioning System and Control Method

A. Selection of Capacitors and Inductors

The passive components of the proposed system are designed with the parameters listed in Table I. The inductor

TABLE I
PV INVERTER PARAMETERS FOR SIMULATIONS

Parameters	Symbol	Value
Power rating	P_n	1 kW
Grid voltage (rms)	V_s	110 V, 60 Hz
PV voltage	V_{MPP}	100 V
Grid inductance	L_{g1}, L_{g2}	500 μH
Output capacitance	C_1, C_2	100 μF
DC-link capacitance	C_{in}	50 μF
Input inductance	L_1, L_2	800 μH
Switching frequency	f_{sw}	10 kHz
Parasitic capacitance	C_{PVg}	110 nF
Resistance of inductor	R_i	0.01Ω
Grounding resistance	R_{GND}	10Ω

values are calculated based on the maximum inductor current and its ripple component, which are given, respectively, by [20]

$$i_{L1,\max} = \frac{V_{in} - \sqrt{V_{in}^2 - 4R_i(-v_{C1})2P_n\left(\frac{v_{C2}-v_{C1}}{V_s^2}\right)}}{2R_i} \tag{28}$$

$$\Delta i_{L1} = \frac{(V_{in} - R_i i_{L1})}{L_1}\frac{1}{2f_{sw}} \tag{29}$$

where $i_{L1,\max}$ is the maximum inductor current, Δi_{L1} is the inductor current ripple, R_i is the internal resistance of the inductor, and f_{sw} is the switching frequency.

The ripple voltage of the capacitor C_1 is given by [20]

$$\Delta v_{C1} = \left|\frac{2P_n(v_{C1}-v_{C2})}{V_s^2 C_1}\right|\frac{1}{2f_s}. \tag{30}$$

The maximum capacitor voltage ripple is chosen to be 1% of the maximum capacitor voltage. Then from (30), C_1 is calculated as 100 μF and C_2 is the same.

B. Control Method for the PV Power Conditioning System

A control block diagram of the PV power conditioning system is shown in Fig. 5, where the DC-link voltage is kept constant and the grid current is regulated to be sinusoidal at unity power factor. For the MPPT algorithm, the P&O (perturb and observe) method is adopted [25].

The transfer function of the PI controller for the DC-link voltage is given by

$$G_{PI} = K_P + \frac{K_I}{s} \tag{31}$$

where K_P and K_I are the proportional and integral gains, respectively. The output of the DC-link voltage controller generates the magnitude of the current reference. The phase

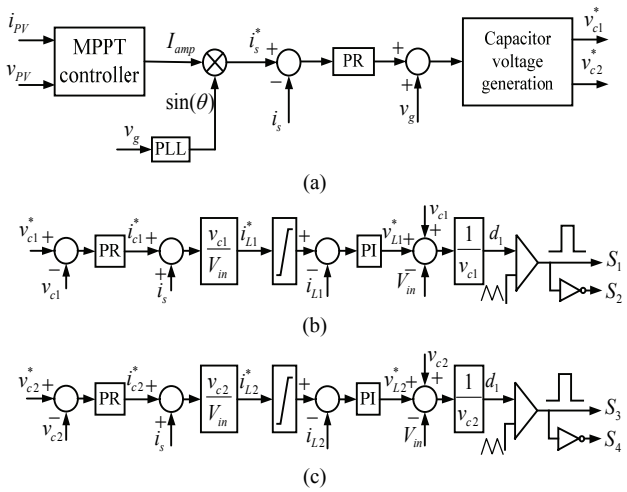

Fig. 5. Control block diagram of a PV power conditioning system. (a) MPPT and grid current control. (b) Capacitor voltage and inductor current control in the upper leg. (c) Capacitor voltage and inductor current control in the lower leg.

angle of the grid voltage is determined by the phase-locked-loop (PLL), which is used for unity power factor operation. To achieve a sinusoidal input current, a proportional-resonant (PR) controller with a feed-forward term of the grid voltage is adopted. The transfer function of the PR controller is expressed as

$$G_{PR} = K_{P1} + \frac{K_{I1}s}{s^2+\omega^2} \tag{32}$$

where K_{P1} and K_{I1} are the proportional gain and the resonant gain, respectively.

For controlling the boost inverter, the output of the current controller is used to generate the voltage references of C_1 and C_2, given in (9) and (10). A cascade-structure of the controllers is adopted, where the inner inductor current control loop and the outer capacitor voltage control loop are included. To control the capacitor voltage, a PR controller is used, as shown in Fig. 5. Next, the inner inductor current control loop is implemented by using a PI controller. Then, the output of the PI controllers is summed with the DC-link voltage, V_{in}, and the capacitor output voltages, v_{c1} and v_{c2}, from which the duty cycles, d_1 and d_2, are determined [19].

V. SIMULATION RESULTS

To validate the feasibility of the proposed circuit, simulations for a 1-kW PV power conditioning system have been carried out, where a solar module in PSIM is adopted. The system parameters are listed in Table I. The PV voltage at the maximum power point is 100-V. It should be noted that only a 50 μF film capacitor is used in the DC-link. The parasitic capacitance (C_{PVg}) is modeled with two capacitors of 110 nF. The grounding resistor (R_G) is 10 Ω. The grid

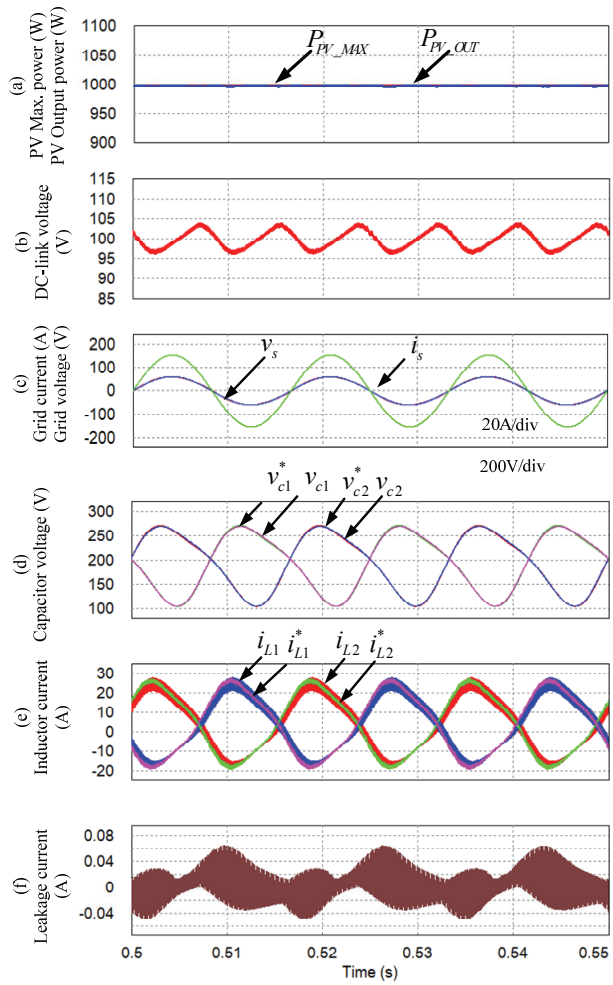

Fig. 6. Control performance of a PV system at the rated power condition. (a) PV maximum power and PV output power. (b) DC-link voltage. (c) Grid current and grid voltage. (d) Capacitor voltages. (e) Inductor currents. (f) Leakage current.

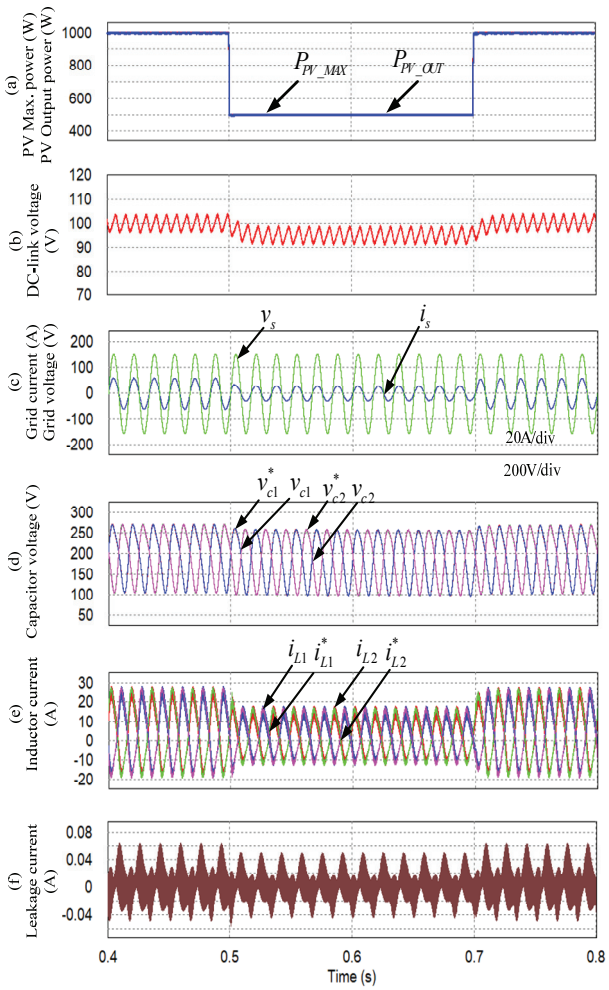

Fig. 7. Responses at a stepwise change in solar irradiance. (a) PV maximum power and PV output power. (b) DC-link voltage. (c) Grid current and grid voltage. (d) Capacitor voltages. (e) Inductor currents. (f) Leakage current.

voltage is 110 V (rms) with a frequency of 60 Hz. The switching frequency is 10 kHz.

Fig. 6 shows the steady-state performance of a PV power conditioning system, where the system is operated at rated power with a solar irradiance of 1 kW/m^2. In Fig. 6(a), it is obvious that the output power accurately tracks the maximum power produced in the PV system. Fig. 6(b) shows the DC-link voltage, where the ripple is about 5% when compared with the MPP voltage value of 100 V. The grid current is shown in Fig. 6(c), which is controlled to be sinusoidal at unity power factor. The capacitor output voltages are shown in Fig. 6(d), in which the actual voltages are regulated toward the references. Fig. 6(e) shows the inductor currents, which are kept close to their references. With the connection of the AC neutral to the negative terminal of the PV through the output capacitor, the leakage current is suppressed. As shown in Fig. 6(f), the leakage current is very low. At 50 mA, it is much lower than the limit of 300 mA [26].

Along with a good steady-state performance, the inverter is also tested in the case of power variations. The transient responses of the inverter are shown in Fig. 7, in which the irradiation is suddenly changed from 1 kW/m^2 to 0.5 kW/m^2. Fig. 7(a) shows the performance of the MPPT control, where the inverter output power is controlled to follow the maximum power produced in the PV system. Fig. 6(b) shows the DC-link voltage at the instant of power change. It can be seen that the DC-link voltage fluctuation is kept stable during the transient condition. The input current is shown in Fig. 7(c), which is still kept sinusoidal at unity power factor. Fig. 6(d) and 6(e) show the control performance of the capacitor voltages and inductor currents in the transient condition, respectively, in which the actual values track their references well. The leakage current of the PV system is shown in Fig. 7(f), where it is also kept at about 60 mA.

The efficiency of the inverter is investigated and compared with other topologies, in which the IGBT HGTG20N60A4, from Fairchild Semiconductor Co., has been used [27]. In this

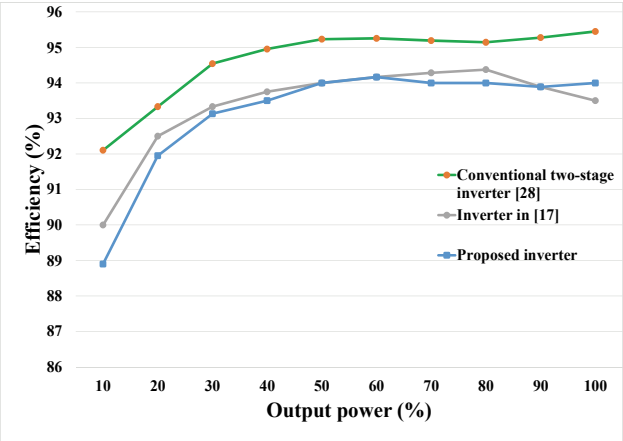

Fig. 8. Efficiency comparison of different converter topologies.

TABLE II
COMPARISON OF VOLTAGE AND CURRENT STRESSES

Converter	Voltage stress	Current stress
Conventional two-stage PV inverter [28]	V_s	$\frac{V_s}{V_{in}} I_s$
Inverter in [17]	$2V_s + V_{in}$	$\frac{(2V_s + V_{in})}{V_{in}} I_s$
Proposed inverter	$V_s + V_{in}$	$\frac{(V_s + V_{in})}{V_{in}} I_s$

analysis, only the power losses of the switching devices are considered. Fig. 8 shows an efficiency comparison for different circuits, where the thermal module of PSIM software was used to analyze the power losses. Due to the higher voltage rating of the switching devices, the efficiency of the proposed inverter is about 1.8% lower than that of the conventional two-stage grid-connected PV inverter [28]. However, the efficiency of the proposed topology is nearly equal to that of the circuit in [17]. In additon, the efficiency of the proposed circuit can be further improved if wide-band-gap devices are employed. The calculated Californian efficiencies [29] for the proposed inverter, the conventional two-stage inverter [28] and the inverter in [17] are obtained as 93.58%, 94.92% and 93.82%, respectively. Since the review of a transformerless PV inverter for leakage current suppression can be found in [7], a similar analysis is not repeated in this work.

In addition, the current and voltage stresses of the proposed inverter are compared with those of existing topologies, which are listed in Table II. The inverter in [17] is operated based on the half-bridge inverter, which requires a high DC voltage at the output of the boost stage. Therefore, this topology has the highest current and voltage stresses. The proposed inverter has lower current and voltage stresses than those of the inverter in [17]. However, it gives higher current and voltage stresses when compared to those of the conventional two-stage inverter [28].

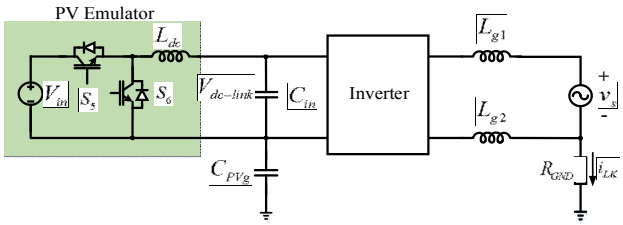

Fig. 9. Configuration of the experimental circuit.

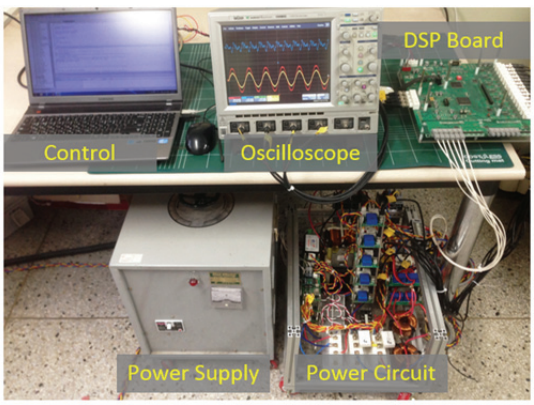

Fig. 10. Hardware set-up.

TABLE III
PV INVERTER PARAMETERS FOR THE EXPERIMENT

Parameters	Symbol	Value
Power rating	P_n	1000 W
Grid voltage (rms)	V_s	110 V, 60 Hz
DC-link voltage	$V_{dc-link}$	100 V
Input voltage	V_{in}	200 V
DC inductance	L_{dc}	2.5 mH
Grid inductance	L_{g1}, L_{g2}	500μH
Output capacitance	C_1, C_2	100 μF
DC-link capacitance	C_{in}	50 μF
Input inductance	L_1, L_2	800 μH
Switching frequency	f_{sw}	10 kHz
Parasitic capacitance	C_{PVg}	110nF
Grounding resistance	R_{RGD}	10Ω

VI. EXPERIMENTAL RESULTS

To show the performance of the proposed PV inverter, a 1-kW prototype was built and tested in the laboratory. Fig. 9 shows the experimental configuration, where the PV panel is emulated by a buck-boost converter, and the input voltage reference for the converter is set to the required output power. Fig. 10 shows the hardware set-up in the laboratory, where the system parameters are listed in Table III. A 32-bit DSP chip (TMS320F28335) was used as the main controller, and a Xilinx FPGA device is employed to generate a switching frequency of 10 kHz.

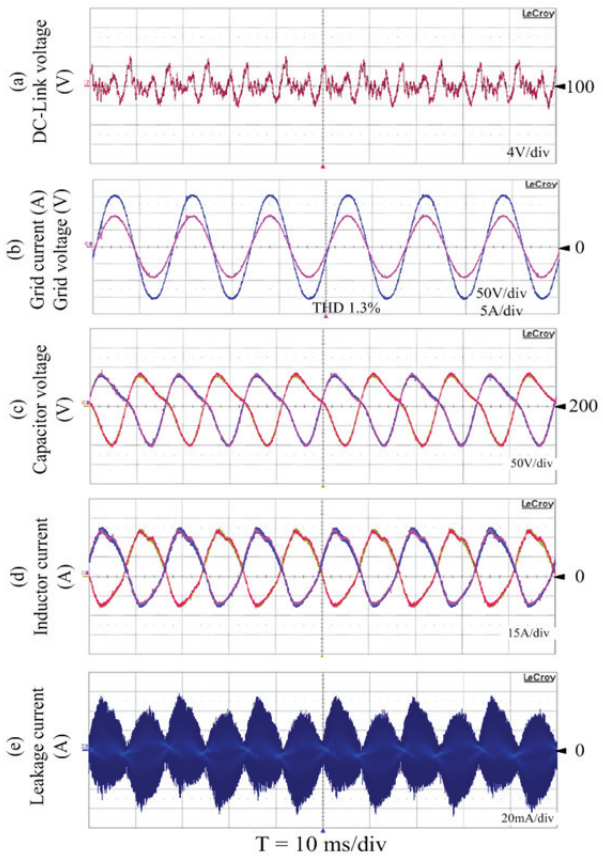

Fig. 11. Control performance under the steady-state condition. (a) DC-link voltage. (b) Grid current and voltage. (c) Capacitor voltages. (d) Inductor currents. (e) Leakage current.

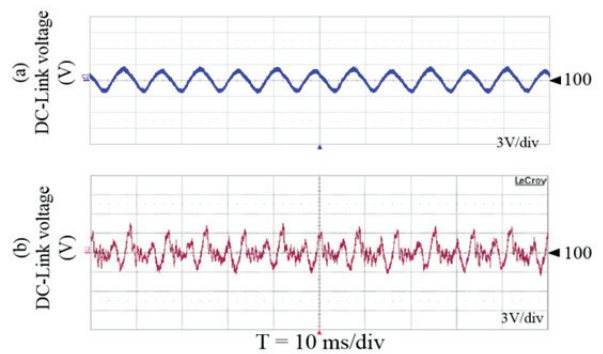

Fig. 12. DC-link voltage waveforms. (a) With a 1,000 μF electrolytic capacitor. (b) With a 50 μF film capacitor.

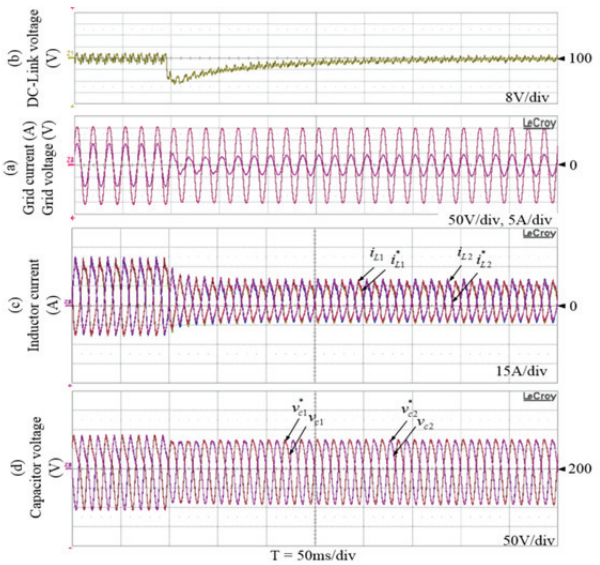

Fig. 13. Responses at a stepwise decrease of power. (a) DC-link voltage. (b) Grid current and grid voltage. (c) Inductor currents. (d) Capacitor voltages.

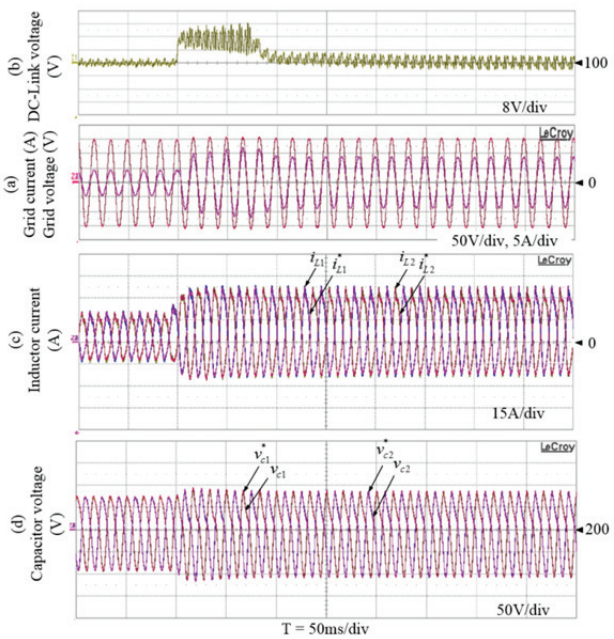

Fig. 14. Responses at a stepwise increase of power. (a) DC-link voltage. (b) Grid current and grid voltage. (c) Inductor currents. (d) Capacitor voltages.

Firstly, Fig. 11 shows the control performance of the proposed scheme under the steady-state condition. Fig. 11(a) shows that the DC-link voltage is kept at its reference of 100V. The grid current and voltage are shown in Fig. 11(b), in which the grid current is controlled to be sinusoidal at a unity power factor. The measured THD of the grid current is about 1.3%. Fig. 11(c) and 11(d) show the control performance of the capacitor voltages and inductor currents, respectively, where the actual values follow their references well. The leakage current of the PV inverter is shown in Fig. 11(d), in which its value is about 60 mA. It is also much lower than the limit of 300 mA.

Next, Fig. 12 shows a comparison of the DC-link voltage ripples between the conventional method with a 1,000μF electrolytic capacitor and the proposed scheme with a 50μF film capacitor. In the conventional method with a large DC-link capacitor, the DC voltage ripple is a little higher than that in the proposed circuit.

Then the PV inverter is tested in the case of power variations. Fig. 13(a) and Fig. 14(a) show the control

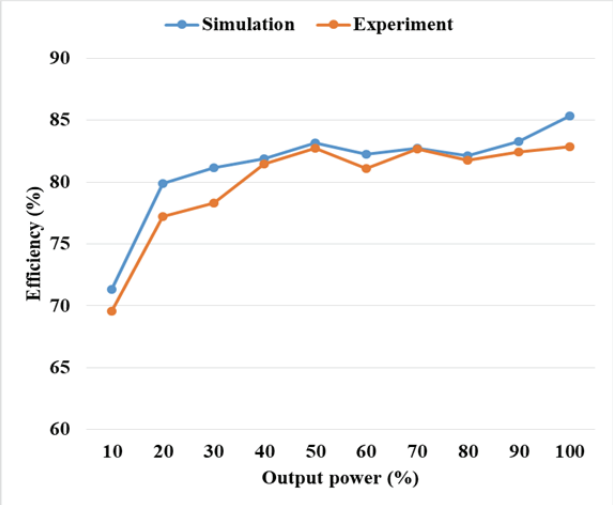

Fig. 15. Measured efficiency of the proposed system.

performance of the inverter for a stepwise decrease and a stepwise increase in power. At the instant of power change, it can be seen that the DC-link voltage fluctuation is kept stable. Fig. 13(b) and Fig. 14(b) show the grid current and voltage in the transient condition. It can be seen that the grid current is kept sinusoidal at a unity power factor. The inductor current control performance is shown in Fig. 13(c) and Fig. 14(c), where the actual currents track their reference well. The output capacitor voltages are well regulated to follow their reference value, as shown in Fig. 13(d) and Fig. 14(d).

Finally, the power loss of the proposed topology was measured by a power meter FLUKE 39, which is shown in Fig. 15. The calculated Californian efficiency is about 81.12%, which is lower than that of the simulation analysis, as shown in Fig. 8, since the IGBT, SKM75GB12T4T from SEMIKRON Co., was used due to limitations of the laboratory facility. In addition, the efficiency of the inverter was estimated by using the thermal module in PSIM, where the same IGBT module used in experiments was also used. It can be seen from Fig. 15 that the efficiencies between simulation and experimental results are very close.

VII. Conclusions

This paper proposed a single-phase transformerless PV power conditioning system based on a boost inverter, where the leakage current can be reduced to 60 mA without any additional devices. In addition, the inverter can effectively solve the inherent pulsating power ripple in single-phase PV inverters by appropriately controlling the output capacitor voltage so that this pulsation component is absorbed by the two output capacitors. Therefore, a 50 μF film capacitor can be used at the DC-link for 1 kW systems, leading to improved reliability and power density of the PV power conditioning system. Simulation and experimental results verified the effectiveness of the proposed topology.

Acknowledgment

This research was supported by the National Research Foundation of Korea (NRF-2014R1A2A1A11052748).

References

[1] Solar Energy Industry Association (SEIA), "U.S. Solar Market Insight: Q2 2016 Report," 2016.

[2] IEA PVPS T1-31:2017, "Snapshot of global photovoltaic markets 2016," pp. 1-16, 2017.

[3] R. Gonzalez, J. Lopez, P. Sanchis, and L. Marroyo, "Transformerless inverter for single-phase photovoltaic systems," *IEEE Trans. Power Electron.*, Vol. 22, No. 2, pp. 693-697, Mar. 2007.

[4] T. Kerekes, R. Teodorescu, M. Liserre, C. Klumpner, and M. Sumner, "Evaluation of three-phase transformerless photovoltaic inverter topologies," *IEEE Trans. Power Electron.*, Vol. 24, No. 9, pp. 2202-2211, Sep. 2009.

[5] W. Chen, X. Yang, W. Zhang, and X. Song, "Leakage current calculation for PV inverter system based on a parasitic capacitor model," *IEEE Trans. Power Electron.*, Vol. 31, No. 12, pp. 8205-8217, Dec. 2016.

[6] Standard VDE 0126-1-1, "Automatic disconnection device between a generator and the public low-voltage grid," 2006.

[7] W. Li, Y. Gu, H. Luo, W. Cui, X. He, and C. Xia, "Topology review and derivation methodology of single-phase transformerless photovoltaic inverters for leakage current suppression," *IEEE Trans. Ind. Electron.*, Vol. 62, No. 7, pp. 4537-4551, Jul. 2015.

[8] J. F. Ardashir, Y. P. Siwakoti, M. Sabahi, S. H. Hosseini, and F. Blaabjerg, "S4 grid-connected single-phase transformerless inverter for PV application," in *IECON Proceedings (Industrial Electronics Conference)*, pp. 2384-2389, 2016.

[9] M. S. Irfan, J. Shin, and J. Park, "New control method for power decoupling of electrolytic capacitor-less photovoltaic micro-inverter with primary side regulation," *J. Electr. Eng. Technol. Technol.*, Vol. 13, No. 2, pp. 1921-1931, Dec. 2017.

[10] M. S. Manoharan, A. Ahmed, and J.-H. Park, "A PV power conditioning system using nonregenerative single-sourced trinary asymmetric multilevel inverter with hybrid control scheme and reduced leakage current," *IEEE Trans. Power Electron.*, Vol. 32, No. 10, pp. 7602-7614, Oct. 2017.

[11] Y.-W. Cho, K.-T. Kim, W.-J. Cha, B.-H. Kwon, and S.-H. Lee, "Evaluation and analysis of transformerless photovoltaic inverter topology for efficiency improvement and reduction of leakage current," *IET Power Electron.*, Vol. 8, No. 2, pp. 255-267, Feb. 2015.

[12] B. Yang, W. Li, Y. Gu, W. Cui, and X. He, "Improved transformerless inverter with common-mode leakage current elimination for a photovoltaic grid-connected power system," *IEEE Trans. Power Electron.*, Vol. 27, No. 2, pp. 752-762, Feb. 2012.

[13] B. Ji, J. Wang, and J. Zhao, "High-efficiency single-phase transformerless PV H6 inverter with hybrid modulation method," *IEEE Trans. Ind. Electron.*, Vol. 60, No. 5, pp. 2104-2115, May 2013.

[14] H. Hu, S. Harb, N. Kutkut, I. Batarseh, and Z. J. Shen, "A

review of power decoupling techniques for microinverters with three different decoupling capacitor locations in PV systems," *IEEE Trans. Power Electron.*, Vol. 28, No. 6, pp. 2711-2726, Jun. 2013.

[15] Y. Sun, Y. Liu, M. Su, W. Xiong, and J. Yang, "Review of active power decoupling topologies in single-phase systems," *IEEE Trans. Power Electron.*, Vol. 31, No. 7, pp. 4778-4794, Jul. 2016.

[16] Y. Tang, W. Yao, P. C. Loh, and F. Blaabjerg, "Highly reliable transformerless photovoltaic inverters with leakage current and pulsating power elimination," *IEEE Trans. Ind. Electron.*, Vol. 63, No. 2, pp. 1016-1026, Feb. 2016.

[17] Y. Xia, J. Roy, and R. Ayyanar, "A capacitance-minimized, doubly grounded transformerless photovoltaic inverter with inherent active-power decoupling," *IEEE Trans. Power Electron.*, Vol. 32, No. 7, pp. 5188-5201, Jul. 2017.

[18] R. O. Caceres and I. Barbi, "A boost DC-AC converter: analysis, design, and experimentation," *IEEE Trans. Power Electron.*, Vol. 14, No. 1, pp. 134-141, Jan. 1999.

[19] P. Sanchis, A. Ursaea, E. Gubia, and L. Marroyo, "Boost DC–AC inverter: A new control strategy," *IEEE Trans. Power Electron.*, Vol. 20, No. 2, pp. 343-353, Mar. 2005.

[20] M. Jang and V. G. Agelidis, "A minimum power-processing-stage fuel-cell energy system based on a boost-inverter with a bidirectional backup battery storage," *IEEE Trans. Power Electron.*, Vol. 26, No. 5, pp. 1568-1577, May 2011.

[21] M. Jang, M. Ciobotaru, and V. G. Agelidis, "A single-stage fuel cell energy system based on a buck-boost inverter with a backup energy storage unit," *IEEE Trans. Power Electron.*, Vol. 27, No. 6, pp. 2825-2834, Jun. 2012.

[22] G.-R. Zhu, S.-C. Tan, Y. Chen, and C. K. Tse, "Mitigation of low-frequency current ripple in fuel-cell inverter systems through waveform control," *IEEE Trans. Power Electron.*, Vol. 28, No. 2, pp. 779-792, Feb. 2013.

[23] D. B. W. Abeywardana Abeywardana, B. Hredzak, and V. G. Agelidis, "A rule-based controller to mitigate DC-side second-order harmonic current in a single-phase boost inverter," *IEEE Trans. Power Electron.*, Vol. 31, No. 2, pp. 1665-1679, Feb. 2016.

[24] H. V. Nguyen and D.-C. Lee, "Reduction of dc-link capacitance for single-phase transformerless PV power conditioning systems," *Futur. Energy Electron. Conf. ECCE Asia (IFEEC 2017 - ECCE Asia)*, pp. 292-297, 2017.

[25] G. He, D. Xu, and M. Chen, "A novel control strategy of suppressing DC current injection to the grid for single-phase PV inverter," *IEEE Trans. Power Electron.*, Vol. 30, No. 3, pp. 1266-1274, Mar. 2015.

[26] Y. Zhou and H. Li, "Analysis and suppression of leakage current in cascaded-multilevel-inverter-based PV systems," *IEEE Trans. Power Electron.*, Vol. 29, No. 10, pp. 5265-5277, Oct. 2014.

[27] "Findchips," 2017. [Online]. Available: https://www.findchips.com/. [Accessed: 01-Jan-2017].

[28] F. Gao, D. Li, P. C. Loh, Y. Tang, and P. Wang, "Indirect DC-link voltage control of two-stage single-phase PV inverter," *2009 IEEE Energy Convers. Congr. Expo. ECCE 2009*, pp. 1166-1172, 2009.

[29] T. K. S. Freddy, N. A. Rahim, Wooi-Ping Hew, and Hang Seng Che, "Comparison and analysis of single-phase transformerless grid-connected PV inverters," *IEEE Trans. Power Electron.*, Vol. 29, No. 10, pp. 5358-5369, Oct. 2014.

Hoang Vu Nguyen was born in Can Tho, Vietnam, in 1990. He received his B.S. degree in Electrical Engineering from Can Tho University, Can Tho, Vietnam, in 2012. He is presently working toward his Ph.D. degree in the Department of Electrical Engineering, Yeungnam University, Gyeongsan, Korea. In 2013, he became a Lecturer in Can Tho University of Technology, Can Tho, Vietnam. His current research interests include AC-DC converters, DC-AC inverters, and electric vehicle chargers.

Do-Hyeon Park was born in Korea, in 1989. He received his B.S. and M.S. degrees in Electrical Engineering from Yeungnam University, Gyeongsan, Korea, in 2015 and 2017, respectively. He is presently working as a Researcher in LC TEK Co. Ltd., Gumi, Korea. His current research interests include motor control.

Dong-Choon Lee received his B.S., M.S. and Ph.D. degrees in Electrical Engineering from Seoul National University, Seoul, Korea, in 1985, 1987, and 1993, respectively. He was a Research Engineer for Daewoo Heavy Industry, Korea, from 1987 to 1988. He has been a faculty member in the Department of Electrical Engineering, Yeungnam University, Gyeongsan, Korea, since 1994. He was a Visiting Scholar in the Power Quality Laboratory, Texas A&M University, College Station, TX, USA, in 1998; the Electrical Drive Center, University of Nottingham, Nottingham, ENG, UK, in 2001; the Wisconsin Electric Machines and Power Electronics Consortium, University of Wisconsin, Madison, WI, USA, in 2004; and the FREEDM Systems Center, North Carolina State University, Raleigh, NC, USA, from September 2011 to August 2012. He was the Editor-in-Chief of the *Journal of Power Electronics* of the Korean Institute of Power Electronics, from January 2015 to December 2017, where he is the Senior Vice President presently. His current research interests include power converter design and control, renewable energy and grid connection, AC machine drives, and power quality.